New Analytical Calculation Models for the Compressive Arch Action in Reinforced Concrete Structures

Xinzheng Lu, Kaiqi Lin, Chenfeng Li, Yi Li

College of Engineering, Swansea University, Swansea SA1 8EN, U.K.

Abstract: Research challenges associated with progressive collapse of reinforced concrete (RC) structures have attracted growing attention from researchers and industries worldwide, since the 1995 explosion at the Murrah Federal Building in Oklahoma City. The Compressive Arch Action (CAA), as a major mechanism to provide structural resistance against progressive collapse resistance under the column removal scenario, has been extensively studied using both experimental and theoretical approaches. However, existing evaluation methods for the CAA resistance are either too complicated or in need of additional information like the peak deformation of the specimen. Another major weakness in the previous CAA calculation methods is the ignorance of the slab effect, which can contribute significantly to the structural resistance. In this study, based on Finite Element (FE) analysis of 50 progressive collapse tests from the literatures and 217 newly designed beam-slab substructures, explicit and easy-to-use CAA calculation models are developed for RC beams with and without slabs. The proposed models are validated by comparing with both experimental and numerical results with an average absolute error less than 10%. The finding from study can provide a quantitative reference for the practical progressive collapse design of RC frame structures.

Keywords: reinforced concrete frame; progressive collapse; compressive arch action; calculation method; slab effect

1 Introduction

Progressive collapse has become an important research frontier since the collapse of Alfred P. Murrah Federal Building in the 1995 Oklahoma City bombing attack (Sozen et al. 1998). Existing researches indicate that the progressive collapse resistance of a structure mainly includes the beam mechanism at small deformation and catenary mechanism at large deformation (Li et al. 2011, 2014a, 2014b; Yu & Tan 2012; Ren et al. 2016; Lu et al. 2016;

Yi et al. 2008; Qian et al. 2014). As such, fully utilizing these two resistance mechanisms has been the primary objective of current progressive collapse design codes (GSA 2013; DoD 2010). According to experimental observations, Compressive Arch Action (CAA) is commonly found in reinforced concrete (RC) beams at small deformations (Yu & Tan 2012, 2013; Ren et al. 2016; Lu et al. 2016; Yi et al. 2008; Qian et al. 2014; Su et al. 2009; Sasani 2011; FarhangVesali et al. 2013; Alogla et al. 2016; Choi & Kim 2011; Sadek et al. 2011). CAA is able to improve the structural resistance by 30% to 150% (Qian et al. 2014 and Su et al. 2009). Therefore, an accurate and easy-to-use calculation method for CAA is of significant value for establishing a rational progressive collapse design.

An illustration of CAA is shown in Figure 1, where the mid-column fails and loses its bearing capacity. The unbalanced gravity load that is originally carried by the failed column gets transformed into a concentrated load P on the beam-column joint. At the early stage, the structural resistance to progressive collapse is provided by the flexural capacities (i.e., M_1 & M_2) of the frame beams (Figure 1a). As the displacement increases, cracking of the concrete will cause a migration of the neutral axis, accompanied by in-plane expansion of the specimen. When the expansion is restrained by the boundaries, CAA will get formed in the beams and enhance the strength of the specimens as shown in Figure 1b. (Rankin & Long 1997).

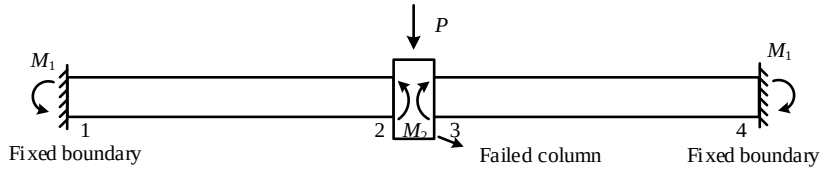

(a) Resistance mechanism of the RC beams at the early stage

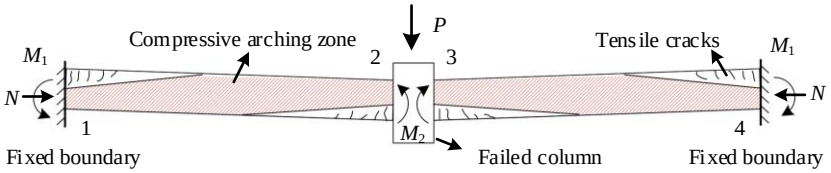

(b) Resistance mechanism of the RC beams at the CAA stage

Figure 1 CAA of the RC beams at small deformation under concentrated load

Many theoretical investigations have been performed to evaluate the CAA resistance, among which Park & Gamble (2000) proposed one of the most widely-accepted CAA

calculation models. The Park & Gamble's model was validated by Su et al. (2009) and Qian et al. (2014) with experimental tests. Afterwards, Yu et al. (2014) and Kang et al. (2017) further updated the Park & Gamble's model, by calculating the force-displacement relationship of RC beams at the CAA stage with a series of iterations. The existing literatures show that the computational models of Park & Gamble (2000), Yu et al. (2014) and Kang et al. (2017) have sufficient accuracy when calculating the CAA resistance of RC frame beams. However, further studies are still needed for the following more involved issues:

(1) Existing models are not suitable for practical use in progressive collapse design: (a) the Park & Gamble's model requires the peak displacement of the CAA, which cannot be easily obtained for real structures; (b) the model proposed by Yu et al. (2014) and Kang et al. (2017) requires a series of iterations to calculate the relative depth of the equivalent compression zone, and the associated computational workload is infeasible without dedicated computer programming.

(2) In real RC frame structures, the frame beams and slabs are always casted together to bear the loads. According to Ren et al. (2016) and Lu et al. (2016), the presence of slab can significantly improve the progressive collapse resistance at the CAA stage. However, existing models can only calculate the CAA of frame beams. In the presence of slabs, the reinforcement on sections 1 to 4 (Figure 1b) will not yield simultaneously, which violates the fundamental assumptions of the existing models and leads to significant evaluation errors.

In order to overcome the limitations of existing calculation models of CAA, we established a series of well-validated finite element (FE) models based on a large database of experimental tests. The sectional stress-strain distributions, key design parameters and their corresponding sensitivities of both beam and beam-slab specimens were analyzed using the FE models. Following the experimental and computational analysis, we proposed explicit and easy-to-use CAA calculation models for RC beams with and without slabs. Comparison with experimental results confirms the new models can accurately obtain the progressive collapse resistance of RC beams (with and without slabs) at the CAA stage. The computational procedure of the new models is simple and easy to implement. This study can

provide a quantitative reference for the practical progressive collapse design of RC frames.

2 The Park & Gamble's model and the database of experiments

2.1 Introduction of the Park & Gamble's Model

The Park & Gamble's model (Park & Gamble 2000) is based on the deformation compatibility and force equilibrium of RC beams under concentrated load. According to the isolated beam model in Figure 2b, the progressive collapse resistance (P) at CAA stage can be expressed as:

$$P = \frac{2\left(M_1 + M_2 - N\delta\right)}{\beta l} \tag{1}$$

where δ is the peak displacement corresponding to the peak load; M_1 and M_2 are the moments at the beam ends; N is the axial force induced by CAA; l is the total length of the two span beam; β is the ratio between the net span and the total span l. Note that M_1, M_2 and N can be derived by calculating the resultant forces at the corresponding cross sections.

In the Park & Gamble's model, the relative depths of the compression zones at sections 1 and 2 are obtained by solving the equations of deformation compatibility and force equilibrium:

$$c' = \frac{h}{2} - \frac{\delta}{4} - \frac{\beta l^2}{4\delta}\left(\varepsilon + \frac{2t}{l}\right) + \frac{T' - T - C_s' + C_s}{1.7 f_c \beta_1 b} \tag{2}$$

$$c = \frac{h}{2} - \frac{\delta}{4} - \frac{\beta l^2}{4\delta}\left(\varepsilon + \frac{2t}{l}\right) - \frac{T' - T - C_s' + C_s}{1.7 f_c \beta_1 b} \tag{3}$$

where c' is the relative depth of the compression zone at section 1; h and b are the height and width of the beam, respectively; ε is the axial compressive strain of the components; t is the translational movement of the boundary; C_c' and C_c are the concrete resultant forces at sections 1 and 2; T', C_s', T and C_s are the reinforcement forces at sections 1 and 2, respectively; f_c is the concrete cylinder strength; β_1 is the ratio of the depth of the equivalent rectangular stress block to the neutral-axis depth, as defined in ACI 318-14 (ACI 2014).

For those RC beams with proper designs, the moments M_1, M_2 and the axial force N can be calculated through combining Equations 2-3 with the stress-strain relationship of the reinforcement and concrete at the ultimate state, after which the CAA resistance P of RC beams can then be readily calculated following Equation 1. The expressions of M_1, M_2 and N

at the beam ends are obtained as:

$$N = C_c + C_s - T = 0.85 f_c \beta_1 cb + C_s - T \tag{4}$$

$$M_1 = 0.85 f_c \beta_1 c' b\left(0.5h - 0.5\beta_1 c'\right) + C_s'(0.5h - d') + T'(0.5h - d') \tag{5}$$

$$M_2 = 0.85 f_c \beta_1 cb\left(0.5h - 0.5\beta_1 c\right) + C_s(0.5h - d') + T(0.5h - d') \tag{6}$$

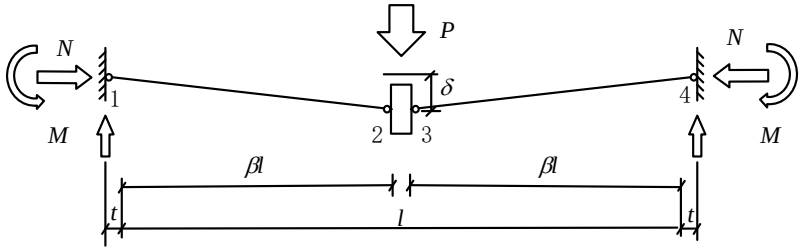

(a) Axially restrained two span RC frame beam under concentrated load

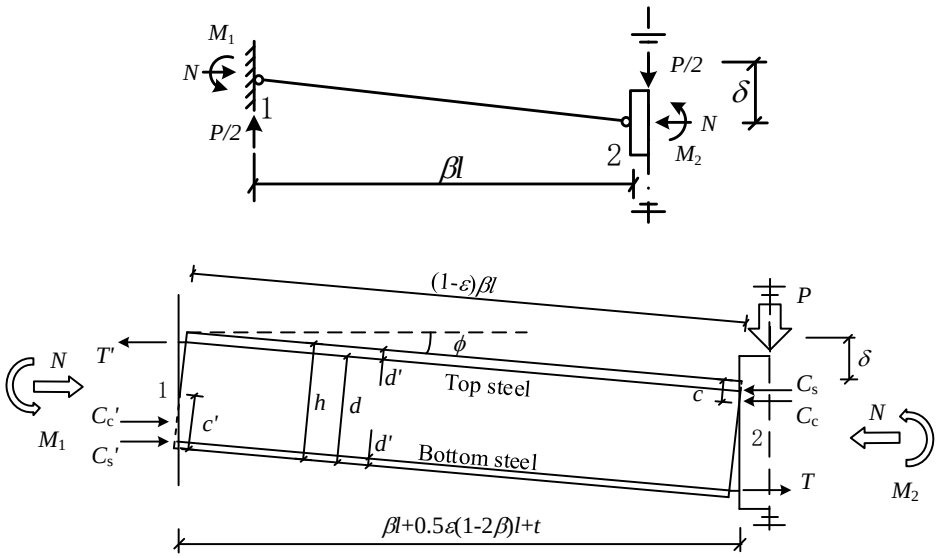

(b) Details of the portion between sections 1 and 2

Figure 2 The Park model

2.2 The database of experiments

Many experiments have been reported to study the progressive collapse of RC frame beams under different column removal scenarios. In order to validate the calculation models of CAA, 50 RC progressive collapse specimens with mid-column removal scenarios are collected in this study. The details of these RC specimens are listed in Appendix A (Yu et al. 2012, 2013; Ren et al. 2016; Qian et al. 2014; Su et la. 2008; Sasani et al. 2011; FarhangVesali et al. 2013; Alogla et al. 2016; Niu et al. 2011; Chen et al. 2010), and among them there are 45 beam specimens and 5 beam-slab specimens. In addition to the specimens

listed in Appendix A, we also reviewed a number of other RC progressive collapse tests found in the literature (e.g., Choi et al. 2011, Sadek et al. 2011, Qian et al. 2012, Prasad & Hutchinson 2014, Lu et al. 2016, Qian et al. 2014 and Dat et al. 2013). However, comparing to the illustrations shown in Figures 1 and 2, these additional tests typically have different boundary conditions or deformation modes, and hence they are not discussed in this work.

2.3 Validation of the Park & Gamble's model

Following the Park & Gamble's model, the CAA resistance P is computed for all 45 beam specimens in Appendix A, and the results are compared with the corresponding experimental measurements. Note that the Park & Gamble's model requires the displacement δ at the peak resistance of CAA, for which the experimentally measured values are adopted in the calculation. The comparisons are shown in Figure 3a, where the average absolute error is 10.97% with a standard deviation of 0.128. This confirms that given the central displacement δ at the peak resistance of CAA, the Park & Gamble's model has sufficient accuracy to calculate the CAA resistance P.

However, for real world structures, it is often hard, if not impossible, to obtain the δ value through experiments, making the Park & Gamble's model impractical in engineering practice. To resolve this situation, Park & Gamble (2000) recommended $\delta = 0.5h$ for use in their calculation procedure. The CAA resistances calculated using the assumption $\delta = 0.5h$ are shown in Figure 3b, where the average absolute error is 20.47% with a standard deviation of 0.158. It is observed that the prediction obtained with $\delta = 0.5h$ significantly underestimates the CAA resistance, and the reduced prediction accuracy poses a major constraint to the practical use of the Park & Gamble's model.

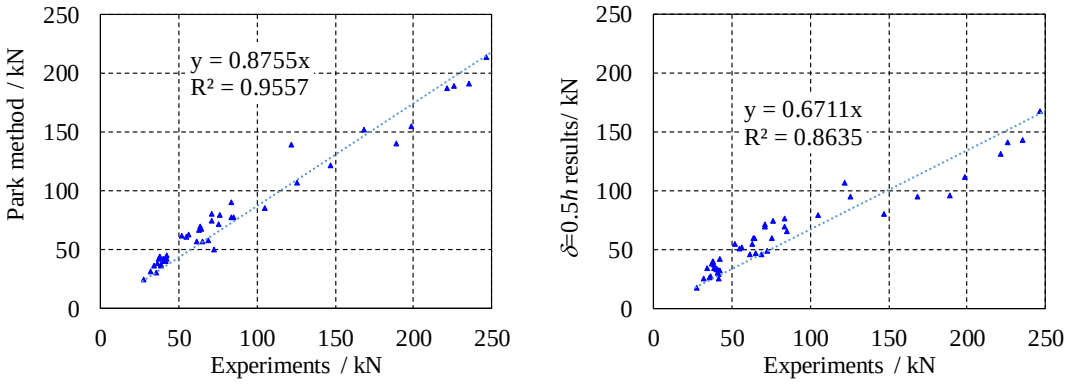

(a) Results obtained with experimentally measured δ

(b) Results obtained with δ=0.5h

Figure 3 Calculation results from the Park & Gamble's model

3 FE models

In order to take a closer examination on the progressive collapse of RC beams, a comprehensive parametric study was then performed using the finite element code OpenSees. Specifically, the fiber-beam element was adopted in the FE analysis, since its feasibility and accuracy in simulating progressive collapse of RC beams have been confirmed in many previous research works (Li et al. 2011, 2014; Ren et al. 2015; Lin et al. 2017; Bao et al. 2008; Talaat et al. 2009; Kazemi-Moghaddam & Sasani 2015). The FE analysis for specimens B1 and S6 (Ren et al. 2016) are taken as an example and plotted in Figures 4a and 4b, where the blue line indicates the FE result and the red line indicates the experiment measurement. For all 45 beam specimens and all 5 beam-slab specimens in Appendix A, the CAA resistances obtained from FE analysis are compared with experimental measurements in Figure 4c, where the average absolute error is 8.34% with a standard deviation of 0.097. Note that the accuracy of the FE model is better than that of the Park & Gamble's model, which justifies the use of the FE model for parametric studies.

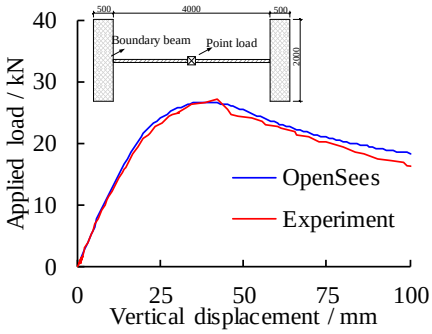

(a) Specimen B1

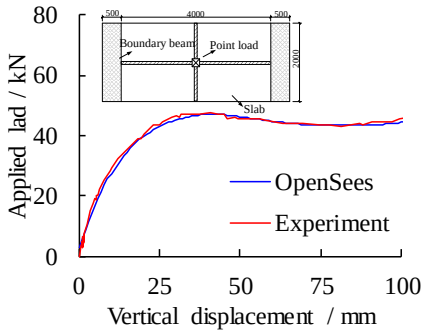

(b) Specimen S6

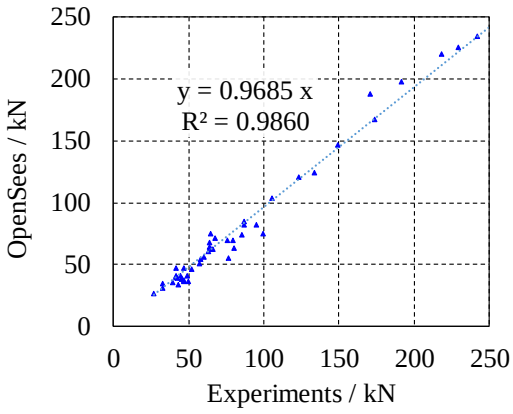

(c) All specimens

Figure 4 Validation of the FE models

4 The new CAA calculation model for beam specimens

As discussed in Sections 2, the practical application of the Park & Gamble's model relies on an erroneous and oversimplified assumption of the peak displacement $\delta = 0.5h$, which introduces significant error to the CAA resistance prediction and limits the usefulness of the model. Through the FE parametric studies, we aim to find a better way to evaluate the δ value, and significantly improve the prediction accuracy of the Park & Gamble's model.

According to the FE results of the 45 beam specimens, three factors are found to affect the value of δ: (1) beam length l (2) beam height h and (3) concrete cylinder strength f_c. Specimen B1 (Figure 4a) tested by Ren et al. (2017) was taken as a prototype to study these key influencing factors. The values of l, h and f_c are changed one-by-one in the FE model of Specimen B1 within the range of 1 m $\leq l \leq$ 5 m, 0.1 m $\leq h \leq$ 0.5 m and 10 MPa $\leq f_c \leq$ 50 MPa, respectively. The results of the parametric study are shown in Figure 5.

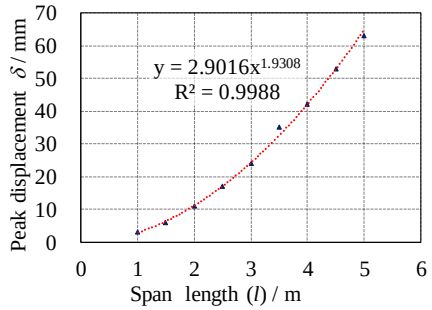

(a) δ–l relationship

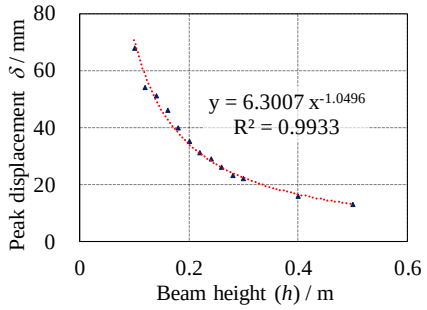

(b) δ–h relationship

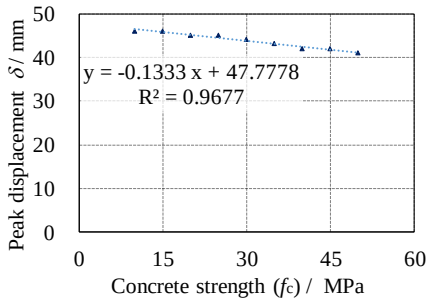

(c) δ–f_c relationship

Figure 5 Parametric study of the peak CAA displacement

It is evident from the parametric study that δ is proportion to l^2, inversely proportion to h, and decrease linearly with the increase of f_c. Note that the influence of f_c can be neglected compared to that of $l^2$and h. Therefore, l^2/h is adopted in this study to predict δ. For the

aforementioned 45 beam specimens, the δ and l^2/h of the FE models are collected and regressed in Figure 6a. The result indicates that δ can be estimated by l^2/h with a satisfactory correlation coefficient (i.e., R^2=0.9459). The equation for δ from the regression is:

$$\delta = 0.0005 l^2 / h \tag{7}$$

Substituting Equation 7 into Equations 1-6, the CAA resistance of RC beams can be predicted. The calculation results are compared with the experimental ones in Figure 6b, where the average absolute error is 8.71% with a standard deviation of 0.107. The proposed model provides a much more accurate prediction of the CAA resistance of RC beams compared to the predictions using the oversimplified assumption $\delta = 0.5h$. Compared to the iterative models proposed by Yu et al. (2014) and Kang et al. (2017), the new model is explicit and avoids completely the time consuming iterations, making it more suitable for engineering practice. In addition, because δ in Equation 7 is estimated using the FE parametric study, which avoids the uncertainties associated with experimental measurement of δ, the results from the proposed model have even smaller errors than the original Park & Gamble's model (Figure 3a).

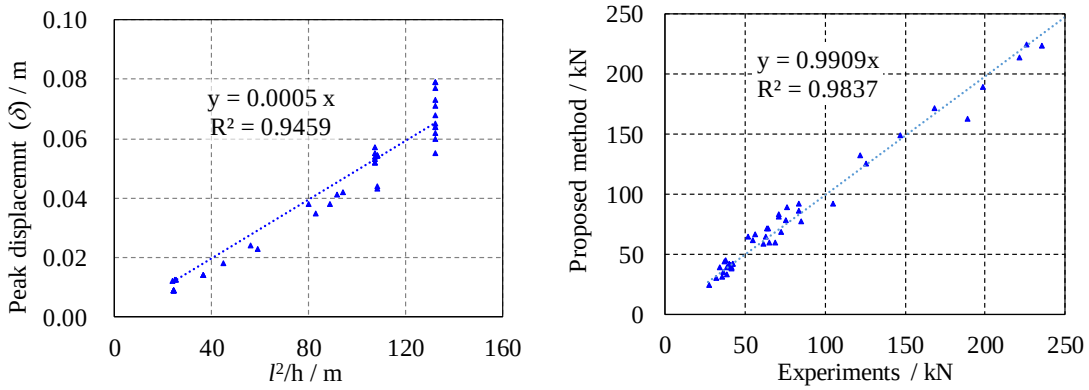

(a) δ~l^2/h relationship (b) Comparison with the experimental results

Figure 6 Validation of the proposed method for the calculation of RC beam specimens

5 The new CAA calculation model for RC beam-slab specimens

As reviewed earlier in Section 1, a major weakness of the Park & Gamble's model is its ignorance of the slab effect. In real structures, the slab is commonly casted together with the underneath beam, and it provides additional resistance to progressive collapse of the structure. The interaction between the beam and the slab and its effect on the CAA resistance can be studied through experimental test and numerical analysis of the beam-slab specimens.

For a beam-slab specimen, the sectional stress-strain distributions of both reinforcement and concrete are more complicated than a beam specimen. Figure 7a shows the force diagram of the beam-slab substructure, while the forces at sections 1 and 2 are illustrated in Figure 7b. The notations in Figure 7 are explained in Table 1. Compared with the beam specimens, the main differences are:

(1) The beam-slab specimen has a T-shaped cross section instead of a rectangular one.

(2) Due to the slab reinforcement, over-reinforced failure occurs at sections 1 and 4 (i.e., the concrete reaches the crush strain before the tensile reinforcement yields) (Ren et al. 2016). On the contrary, at sections 2 and 3, the tensile reinforcement yields at the early stage of the loading procedure but the compressive reinforcement might not yield at the peak resistance of CAA. The assumption in the Park & Gamble's model that both concrete and reinforcement reach their ultimate state is no longer applicable for a beam-slab specimen, and as a result the forces M_1, M_2 and N at the beam ends in Equation 1 cannot be directly calculated.

(3) The proposed model for the peak displacement δ of CAA, i.e. Equation 7, has a high accuracy for the regular beam specimen but not suitable for the T-shaped beam-slab specimen.

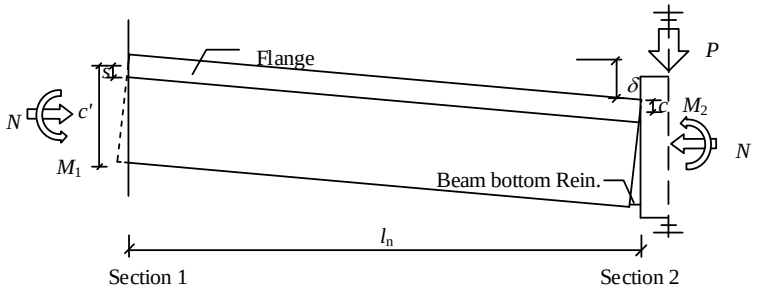

(a) Half portion of the beam-slab specimen

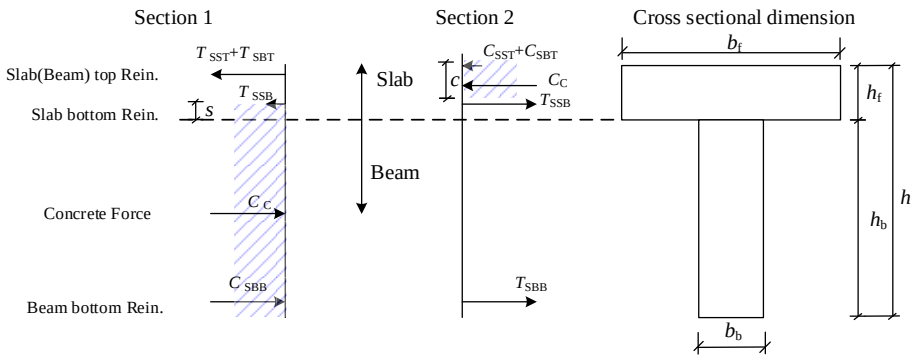

(b) Force distribution at typical sections

Figure 7 Diagram of the beam-slab specimen at CAA

Table 1 Definition of symbols in Figure 7

Symbol	Meaning
T'_{SST}	Tensile force of the top slab reinforcement at section 1
T'_{SBT}	Tensile force of the top beam reinforcement at section 1
T'_{SSB}	Tensile force of the bottom slab reinforcement at section 1
C'_{C}	Compressive force of concrete at section 1
C'_{SBB}	Compressive force of the bottom beam reinforcement at section 1
c'	Height of the concrete compressive zone at section 1
s	Height of the concrete compressive zone in slab at section 1
C_{SST}	Compressive force of the top slab reinforcement at section 2
C_{SBT}	Compressive force of the top beam reinforcement at section 2
T_{SSB}	Tensile force of the bottom slab reinforcement at section 2
C_{C}	Compressive force of concrete at section 2
T_{SBB}	Tensile force of the bottom beam reinforcement at section 2
c	Height of the concrete compressive zone at section 2
d'	Thickness of the concrete cover
h_f	Slab thickness
h_b	Beam height minus slab thickness
b_f	Slab width
b_b	Beam width
l_n	Net span

In order to have a rough idea about the limitation of the Park & Gamble's model (which assumes all reinforcements yield), we directly applied the standard calculation procedure to the beam-slab specimens tested by Ren et al. (2016) and compared the peak resistance prediction with the experimental measurement. As shown in Figure 8, the average absolute error is 18.7%, and for about two thirds of the specimens the errors exceed 20%, which makes the Park & Gamble's model unfeasible in this situation.

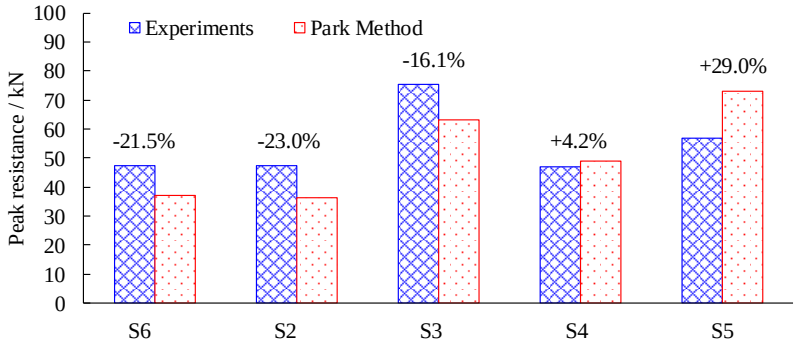

Figure 8 Comparison between the experimental results and the Park & Gamble's model

for beam-slab specimens

5.1 Parametric study of beam-slab specimens using FE models

The validation described in Section 3 has proved the FE models are capable of simulating the behavior of beam-slab specimens at the CAA stage with a good accuracy. Due to the limited number of beam-slab experiments in the literature, we performed a comprehensive parametric study of beam-slab specimens using the validated FE model, where a series of RC beam-slab substructures with commonly used dimensions are designed according to the Chinese Code for the Design of Concrete Structures (MOHURD 2010). The design parameters of these beam-slab substructures are listed in Table 2. The 6-story and 4-bay RC frame used by Ren et al. (2016), Lu et al. (2017) and Lin et al. (2017) is taken as the prototype building. The dead load and live load on the floor are 5.0 kN/m^2 and 2.0 kN/m^2, respectively. For each individual design, only one design parameter is changed according to the values listed in Table 2. In total, 217 models with different span lengths, beam heights, beam widths, slab thicknesses and slab widths are derived based on the MOHURD 2010 code and analysed using the validated FE model.

Table 2 Design parameters of different beam-slab models

Design parameter	Value range		
Span length / m	4	6	8
Beam height / m	0.4/0.5	0.5/0.6/0.7	0.7/0.8/0.9/1.0
Beam width / m	0.2/0.25	0.2/0.25/0.3/0.35	0.2/0.3/0.4/0.5
Slab thickness / m	0.08/0.12/0.16	0.08/0.12/0.16	0.12/0.16
Slab width / m	1.33/2.67/4	2.0/4.0/6.0	2.67/5.34/8.0

5.2 Analysis of typical cross sections

For the beam-slab substructure, sections 1 and 2 are chosen as the typical cross sections as shown in Figure 7b. According to previous analysis, at the point of peak CAA resistance: (1) the bottom beam reinforcement at section 1 yields under compression, while the depth of the compressive zone of concrete and the forces of the slab reinforcement and the top beam reinforcement are unknown; (2) the bottom beam reinforcement at section 2 yields under tension, while the depth of the concrete compressive zone and the forces of the slab reinforcement and the top beam reinforcement are unknown. Hence, to calculate the CAA resistance of beam-slab substructures, the following parameters need to be specified:

(1) Parameters for Section 1:

(a) The depth of the concrete compressive zone in the slab (i.e., s). Note that $s < 0$ indicates that the concrete compressive zone locates only at the beam web section.

(b) The tensile force of the bottom slab reinforcement (i.e., T'_{SSB}).

(c) The tensile forces of the top slab and the top beam reinforcements (i.e., T'_{SST} and T'_{SBT}). For simplicity, it is assumed that the top slab and the top beam reinforcements are at the same height. Assuming the plane sections remain plane, the strains of the top slab and the top beam reinforcement remain the same.

(2) Parameters for Section 2:

(a) The depth of the concrete compressive zone in the slab (i.e., c). Note that $c > h_f$ indicates that part of the concrete compressive zone locates at the beam web section.

(b) The tensile force of the bottom slab reinforcement (i.e., T_{SSB}).

(c) The compressive forces of the top slab and the top beam reinforcements (i.e., C_{SST} and C_{SBT}). Assuming the plane sections remain plane, the strains of the top slab and the top beam reinforcements remain the same.

Let $\sigma_s=\kappa_i f_y$ denote the stress levels of the reinforcement at different sections, where κ_i is the reinforcement stress coefficient at section i and f_y is the yield stress of the reinforcement. The stresses of the reinforcement at sections 1 and 2 of the 217 beam-slab FE models at the peak resistance of CAA are shown in Figure 9.

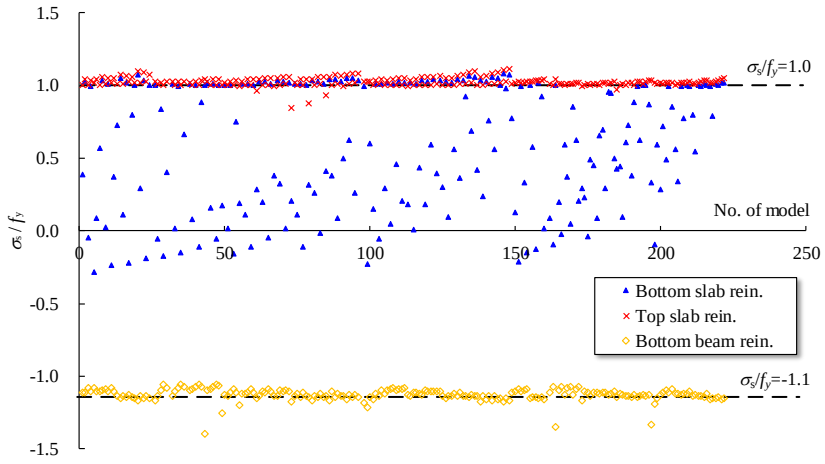

(a) Reinforcement stress levels at section 1

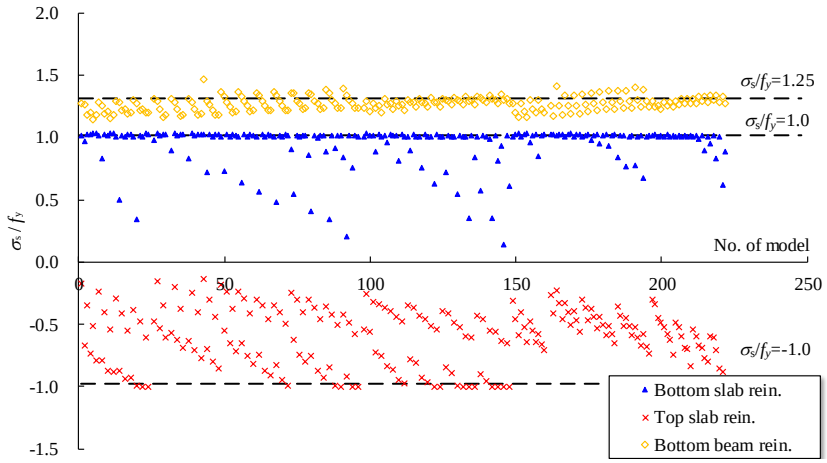

(b) Reinforcement stress levels at section 2

Figure 9 Stress levels of the reinforcement at sections 1 and 2 of the FE models

The FE results indicate the bottom beam reinforcement yields under compression at section 1 when the beam-slab substructures reach their peak CAA resistance. The top slab reinforcement yields under tension, while the yielding status of the bottom slab reinforcement depends on the ratio between the area of the upper slab and the bottom beam (i.e., $b_b h_b / b_f h_f$). The relation between σ_s / f_y and $b_b h_b / b_f h_f$ is shown in Figure 10a (σ_s is the stress of the bottom slab reinforcement), from which the following equations can be derived:

$$\begin{cases} \kappa_{1SSB} = 1.0, & \text{when } b_b h_b / b_f h_f \geq 0.45 \\ \kappa_{1SSB} = 3.13 b_b h_b / b_f h_f - 0.41, & \text{when } b_b h_b / b_f h_f < 0.45 \end{cases} \quad (8)$$

Similarly, for section 2, the following equations can be derived from Figure 10b:

$$\begin{cases} \kappa_{2SSB} = -1.25 b_b h_b / b_f h_f + 1.75, & \text{when } b_b h_b / b_f h_f \geq 0.6 \\ \kappa_{2SSB} = 1.0, & \text{when } b_b h_b / b_f h_f < 0.6 \end{cases} \quad (9$$

$$\kappa_{2SST} = \kappa_{2SBT} = 0.6 \quad (10)$$

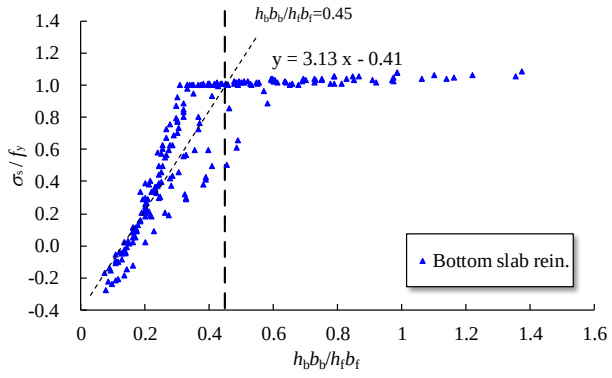

(a) Section 1

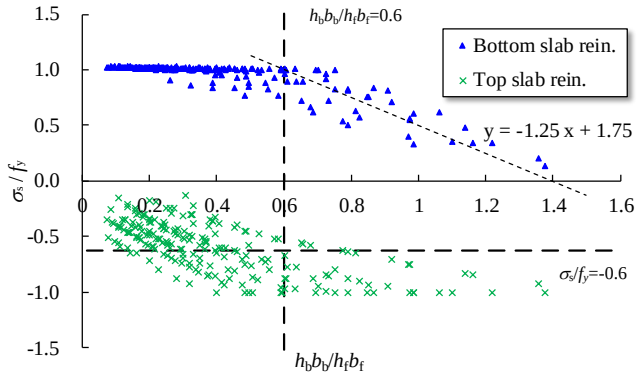

(b) Section 2

Figure 10 Approximation for stress level of the reinforcement

In order to calculate the resultant moments and axial forces at the beam ends, the depths of the concrete compressive zone (i.e., c and s) need to be specified. For the axial restrained beam-slab substructure with fixed boundaries as shown in Figure 7a, the following relation can be derived through deformation compatibility of the beams:

$$c' + c = h_{\mathrm{b}} + s + c = h - \frac{\delta}{2} \tag{11}$$

Equation 11 can also be written as:

$$s + c = h - h_{\mathrm{b}} - \frac{\delta}{2} = h_{\mathrm{f}} - \frac{\delta}{2} \tag{12}$$

According to the cross sectional analysis in Figure 7b:

$$C'_{\mathrm{C}} + C'_{\mathrm{SBB}} - \left(T'_{\mathrm{SST}} + T'_{\mathrm{SBT}} + T'_{\mathrm{SSB}}\right) = C_{\mathrm{C}} + C_{\mathrm{SST}} + C_{\mathrm{SBT}} - \left(T_{\mathrm{SSB}} + T_{\mathrm{SBB}}\right) \tag{13}$$

Previous reinforcement stress analyses shows that in most cases the bottom slab reinforcement at section 1 is under compression, which implies that the concrete at the beam web is also under compression. Therefore, according to Figure 7 and ACI318-14 (ACI 2014), it can be derived that:

$$C'_{\mathrm{C}} - C_{\mathrm{C}} = f_{\mathrm{c}} h_{\mathrm{b}} b_{\mathrm{b}} + 0.85 f_{\mathrm{c}} \beta_1 b_{\mathrm{f}} s - 0.85 f_{\mathrm{c}} \beta_1 b_{\mathrm{f}} c \tag{14}$$

Substituting Equation 14 into Equation 12 yields:

$$\begin{aligned} &f_{\mathrm{c}} h_{\mathrm{b}} b_{\mathrm{b}} + 0.85 f_{\mathrm{c}} \beta_1 b_{\mathrm{f}} s - 0.85 f_{\mathrm{c}} \beta_1 b_{\mathrm{f}} c = \\ &T'_{\mathrm{SST}} + T'_{\mathrm{SBT}} + T'_{\mathrm{SSB}} - C'_{\mathrm{SBB}} + C_{\mathrm{SST}} + C_{\mathrm{SBT}} - T_{\mathrm{SSB}} - T_{\mathrm{SBB}} \end{aligned} \tag{15}$$

Based on the previous analysis, the resultant force of the reinforcement can be written as:

Section 1:

$$T'_{\mathrm{SST}} = f_{\mathrm{yst}}A_{\mathrm{st}}\,,\quad T'_{\mathrm{SBT}} = f_{\mathrm{ybt}}A_{\mathrm{bt}}\,,\quad C'_{\mathrm{SBB}} = f_{\mathrm{ybb}}A_{\mathrm{bb}}$$

$$T'_{\mathrm{SSB}} = \begin{cases} f_{\mathrm{ysb}}\mathrm{A}_{\mathrm{sb}} & b_{\mathrm{b}}h_{\mathrm{b}}/b_{\mathrm{f}}h_{\mathrm{f}} \geq 0.45 \\ f_{\mathrm{ysb}}\mathrm{A}_{\mathrm{sb}}\left(3.13b_{\mathrm{b}}h_{\mathrm{b}}/b_{\mathrm{f}}h_{\mathrm{f}} - 0.41\right) & b_{\mathrm{b}}h_{\mathrm{b}}/b_{\mathrm{f}}h_{\mathrm{f}} < 0.45 \end{cases} \tag{16}$$

Section 2:

$$T_{\mathrm{SBB}} = f_{\mathrm{ybb}}A_{\mathrm{bb}}\,,\quad C_{\mathrm{SST}} = 0.6\,f_{\mathrm{yst}}A_{\mathrm{st}}\,,\quad C_{\mathrm{SBT}} = 0.6\,f_{\mathrm{ybt}}A_{\mathrm{bt}}$$

$$T_{\mathrm{SSB}} = \begin{cases} f_{\mathrm{ysb}}\mathrm{A}_{\mathrm{sb}} & b_{\mathrm{b}}h_{\mathrm{b}}/b_{\mathrm{f}}h_{\mathrm{f}} \leq 0.6 \\ f_{\mathrm{ysb}}\mathrm{A}_{\mathrm{sb}}\left(-1.25b_{\mathrm{b}}h_{\mathrm{b}}/b_{\mathrm{f}}h_{\mathrm{f}} + 1.75\right) & b_{\mathrm{b}}h_{\mathrm{b}}/b_{\mathrm{f}}h_{\mathrm{f}} > 0.6 \end{cases} \tag{17}$$

where f_{y} and A are the yield stress and the reinforcement area, respectively.

Equation 15 can also be written as:

$$s - c = \frac{T'_{\mathrm{SST}} + T'_{\mathrm{SBT}} + T'_{\mathrm{SSB}} - C'_{\mathrm{SBB}} + C_{\mathrm{SST}} + C_{\mathrm{SBT}} - T_{\mathrm{SSB}} - T_{\mathrm{SBB}} - f_{\mathrm{c}}h_{\mathrm{b}}b_{\mathrm{b}}}{0.85\,f_{\mathrm{c}}\beta_1 b_{\mathrm{f}}} \tag{18}$$

The heights of the concrete compression zone at different sections can be obtained by combining Equations 12 and 18:

$$s = \frac{h_{\mathrm{f}}}{2} - \frac{\delta}{4} + \frac{T'_{\mathrm{SST}} + T'_{\mathrm{SBT}} + T'_{\mathrm{SSB}} - C'_{\mathrm{SBB}} + C_{\mathrm{SST}} + C_{\mathrm{SBT}} - T_{\mathrm{SSB}} - T_{\mathrm{SBB}} - f_{\mathrm{c}}h_{\mathrm{b}}b_{\mathrm{b}}}{1.7\,f_{\mathrm{c}}\beta_1 b_{\mathrm{f}}} \tag{19}$$

$$c = \frac{h_{\mathrm{f}}}{2} - \frac{\delta}{4} - \frac{T'_{\mathrm{SST}} + T'_{\mathrm{SBT}} + T'_{\mathrm{SSB}} - C'_{\mathrm{SBB}} + C_{\mathrm{SST}} + C_{\mathrm{SBT}} - T_{\mathrm{SSB}} - T_{\mathrm{SBB}} - f_{\mathrm{c}}h_{\mathrm{b}}b_{\mathrm{b}}}{1.7\,f_{\mathrm{c}}\beta_1 b_{\mathrm{f}}} \tag{20}$$

Substituting s and c into the following equations gives the concrete resultant compressive force at sections 1 and 2:

$$C'_{\mathrm{C}} = f_{\mathrm{c}}h_{\mathrm{b}}b_{\mathrm{b}} + 0.85\,f_{\mathrm{c}}\beta_1 b_{\mathrm{f}}s \tag{21}$$

$$C_{\mathrm{C}} = 0.85\,f_{\mathrm{c}}\beta_1 b_{\mathrm{f}}c \tag{22}$$

As both concrete and reinforcement forces are specified, the resultant forces at sections 1 and 2 (N, M_1 and M_2) can be calculated as:

$$N = C'_{\mathrm{C}} + C'_{\mathrm{SBB}} - \left(T'_{\mathrm{SST}} + T'_{\mathrm{SBT}} + T'_{\mathrm{SSB}}\right) \tag{23}$$

$$\begin{aligned} M_1 = {} & -0.85\,f_{\mathrm{c}}\beta_1 b_{\mathrm{f}}s\left(h_{\mathrm{b}} - 0.5h + 0.5\beta_1 s\right) + 0.5\,f_{\mathrm{c}}h_{\mathrm{b}}b_{\mathrm{b}}h_{\mathrm{f}} + \\ & \left(T'_{\mathrm{SST}} + T'_{\mathrm{SBT}} + C'_{\mathrm{SBB}}\right)(0.5h - d') + T'_{\mathrm{SSB}}(0.5h + d' - h_{\mathrm{f}}) \end{aligned} \tag{24}$$

$$\begin{aligned} M_2 = {} & 0.85\,f_{\mathrm{c}}\beta_1 b_{\mathrm{f}}c\left(0.5h - 0.5\beta_1 c\right) + \\ & \left(C_{\mathrm{SST}} + C_{\mathrm{SBT}} + T_{\mathrm{SBB}}\right)(0.5h - d') - T_{\mathrm{SSB}}(0.5h + d' - h_{\mathrm{f}}) \end{aligned} \tag{25}$$

Finally, the progressive collapse resistance of beam-slab substructure at the CAA stage can be obtained by substituting N, M_1 and M_2 into Equation 1.

5.3 Estimating the peak displacement of CAA for beam-slab substructures

Similar to the calculation procedure of RC beams, the calculation of beam-slab substructures also requires the peak displacement (i.e., δ) of CAA in Equation 1. Following a similar analysis as shown in Figures 5 and 6, the geometries of all 217 beam-slab models are used to regress δ and the following equation is obtained:

$$\delta = 0.000276 \times \left(0.0023 \times \left(\frac{b_f}{b_b} \right) + 0.9875 \right) \times \left(\frac{l^2}{h_f + 0.5 h_b} \right) \tag{26}$$

where h, b_b and h_f are defined as in Table1, and l is the total span. As shown in Figure 11, a good agreement is observed between the above prediction and the FE results.

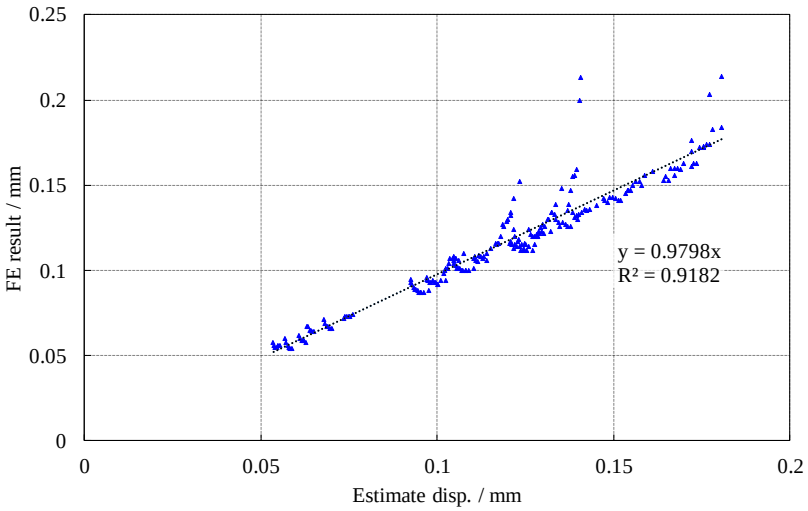

Figure 11 Comparison of the predicted δ by Equation 26 and the FE results

5.4 Validation of the accuracy of the proposed model

Based on the δ predicted in Equation 26, the calculation procedure in Section 5.2 (i.e., Equations 19 to 25) can be used to calculate the CAA resistance of the beam-slab specimens. Specimens S6 tested by Ren et al. (2016) is taken as an example to illustrate the calculation procedure of the proposed model, and the details are shown in Appendix B. For all 217 beam-slab model designed in this study, the comparison between the proposed model and the FE results is provided in Figure 12a, where the average absolute error is 6.25% with a standard deviation of 0.064. For the five one-way beam-slab specimens tested by Ren et al. (2016), the calculation results are compared with the FE and experimental results in Figure

12b, where the average absolute estimating error is 9.28%. These comparisons confirm that the proposed explicit method is able to obtain accurately the CAA resistance of beam-slab specimens.

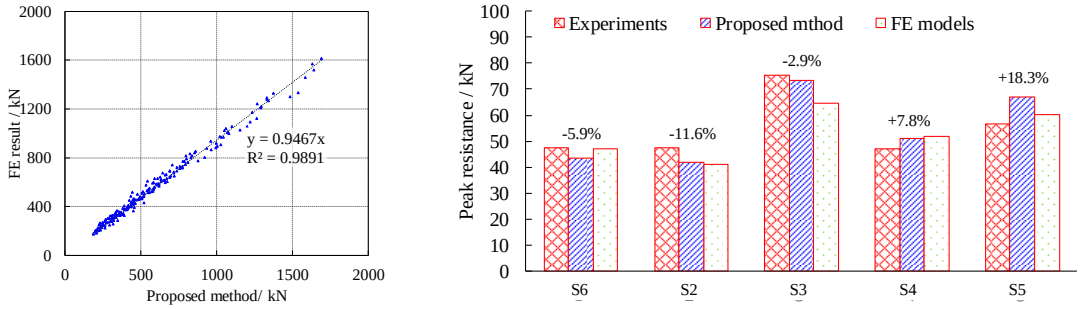

(a) Comparison with FE results (b) Comparison with the experiments tests by Ren et al. (2016)

Figure Validation of the proposed model for 12 beam-slab specimens

6 Conclusion

Compressive arch action serves as the major mechanism to resist progressive collapse in RC frames at small deformation. An accurate and efficient model to calculate the CAA resistance has significant value to the progressive collapse design of RC structures. Existing models can neither meet the engineering practices demands, nor calculate the CAA resistance of beam-slab specimens. Based on a database of 45 beam specimens and 5 beam-slab specimens, and the FE analysis of 45 beam specimens and 217 beam-slab substructures, explicit and practical calculation models of CAA for RC beams with and without slabs are proposed in this study. The main conclusions are:

(1) This study proposes a simple and explicit method that is able to calculate the CAA resistance of RC beams based on the geometric and reinforcement information. The equations to predict the peak displacement of CAA is proposed based on the regression of the FE results of 45 experimental specimens. The predicted CAA resistance is more accurate than the Park & Gamble's model.

(2) A set of 217 beam-slab substructures with the most commonly used span length, beam height, beam width, slab thickness and slab width in engineering practice are designed. The sectional stresses of concrete and reinforcement of beam-slab substructures under CAA are proposed based on the FE results of these 217 beam-slab substructures, which establishes a foundation for the calculation model of CAA of beam-slab substructures.

(3) The explicit CAA resistance calculation model, as well as the corresponding peak

displacement estimating method, for beam-slab substructures is proposed. The comparison with both FE and experimental results confirms the proposed explicit model is able to calculate accurately the CAA resistance of RC beam-slab substructures.

Acknowledgement

The authors are grateful for the financial support received from the National Natural Science Foundation of China (No. 51778341), and the European Community's Seventh Framework Programme (Marie Curie International Research Staff Exchange Scheme, Grant No. 612607) and the Sêr Cymru National Research Network in Advanced Engineering and Materials.

References

Alogla, K., Weekes, L., & Augusthus-Nelson, L. (2016). A new mitigation scheme to resist progressive collapse of RC structures. Construction and Building Materials, 125, 533-545.

American Concrete Institute (ACI). (2014). Building code requirements for structural concrete (ACI 318-14) and commentary (318R-14). Detroit, MI.

Bao, Y., Kunnath, S. K., El-Tawil, S., & Lew, H. S. (2008). Macromodel-based simulation of progressive collapse: RC frame structures. Journal of Structural Engineering, 134(7), 1079-1091.

Chen MH, Song XS, Su YP (2010). Influence of reinforcement ratio on ultimate bearing capacity of rein-forced concrete frame beams: test study on arch action. Journal of Natural Disasters, 1, 44-48. (in Chinese)

Choi, H., & Kim, J. (2011). Progressive collapse-resisting capacity of RC beam–column sub-assemblage. magazine of concrete research, 63(4), 297-310.

Department of Defense (DoD). (2010). Design of structures to resist progressive collapse. Unified facility criteria, UFC 4-023-03, Washington, DC.

Dat, P. X., & Tan, K. H. (2013). Experimental study of beam–slab substructures subjected to a penultimate-internal column loss. Engineering Structures, 55, 2-15.

FarhangVesali, N., Valipour, H., Samali, B., & Foster, S. (2013). Development of arching

action in longitudinally-restrained reinforced concrete beams. Construction and Building Materials, 47, 7-19.

General Services Administration (GSA). (2013). Alternate path analysis and design guidelines for progressive collapse resistance. Washington, DC.

Sozen, M., Thornton, C., Corley, W., and Sr., P. (1998). The Oklahoma City Bombing: structure and mechanisms of the Murrah Building. Journal of Performance of Constructed Facilities, 12(3), 120–136.

Kang, S. B., & Tan, K. H. (2017). Analytical study on reinforced concrete frames subject to compressive arch action. Engineering Structures, 141, 373-385.

Kazemi-Moghaddam, A., & Sasani, M. (2015). Progressive collapse evaluation of Murrah Federal Building following sudden loss of column G20. Engineering Structures, 89, 162-171.

Li Y, Lu XZ, Guan H, Ye LP, An improved tie force method for progressive collapse resistance design of reinforced concrete frame structures, Engineering Structures, 2011, 33(10): 2931-2942.

Li Y, Lu XZ, Guan H, Ye LP, An energy-based assessment on dynamic amplification factor for linear static analysis in progressive collapse design of ductile RC frame structures, Advances in Structural Engineering, 2014, 17(8): 1217-1225.

Li Y, Lu XZ, Guan H, Ye LP, Progressive collapse resistance demand of RC frames under catenary mechanism, ACI Structural Journal, 2014, 111 (5), 1225-1234.

Lin KQ, Li, Y, Lu XZ, Guan H, Effects of seismic and progressive collapse designs on the vulnerability of RC frame structures. Journal of Performance of Constructed Facilities-ASCE, 2017, 31(1): 04016079. DOI: 10.1061/(ASCE)CF.1943-5509.0000942.

Lu, X., Lin, K., Li, Y., Guan, H., Ren, P., & Zhou, Y. (2016). Experimental investigation of RC beam-slab substructures against progressive collapse subject to an edge-column-removal scenario. Engineering Structures.

Ministry of Housing and Urban-Rural Development of the People's Republic of China (MOHURD). (2010a). "Code for design of concrete structures." GB50010-2010, Beijing, China.

Niu JX, Su YP, Wang HX (2011). Tentative studies on collapse resistance capacity of

reinforced concrete frame beam. Proceeding of the 20th National Conference on Structural Engineering. Beijing: Engineering Mechanics Press, 377-382 (in Chinese)

Prasad S, Hutchinson T C. Evaluation of older reinforced concrete floor slabs under corner support failure. ACI Structural Journal, 2014, 111(4): 839-849.

Park, R., & Gamble, W. L. (2000). Reinforced concrete slabs. John Wiley & Sons.

Qian K, Li B. Slab effects on response of reinforced concrete substructures after loss of corner column. ACI Structural Journal, 2012, 109(6): 845-855.

Qian, K., Li, B., & Ma, J. X. (2014). Load-carrying mechanism to resist progressive collapse of RC buildings. Journal of Structural Engineering, 141(2), 04014107.

Rankin, G. I. B., & Long, A. E. (1997). Arching action strength enhancement in laterally-restrained slab strips. Proceedings of the Institution of Civil Engineers-Structures and Buildings, 122(4), 461-467.

Ren PQ, Li Y, Guan H, Lu XZ, Progressive collapse resistance of two typical high-rise RC frame shear wall structures, Journal of Performance of Constructed Facilities-ASCE, 2015, 29(3), 04014087.

Ren, P., Li, Y., Lu, X., Guan, H., & Zhou, Y. (2016). Experimental investigation of progressive collapse resistance of one-way reinforced concrete beam–slab substructures under a middle-column-removal scenario. Engineering Structures, 118, 28-40.

Sadek, F., Main, J. A., Lew, H. S., & Bao, Y. (2011). Testing and analysis of steel and concrete beam-column assemblies under a column removal scenario. Journal of Structural Engineering, 137(9), 881-892.

Sasani, M., Werner, A., & Kazemi, A. (2011). Bar fracture modeling in progressive collapse analysis of reinforced concrete structures. Engineering Structures, 33(2), 401-409.

Sozen, M., Thornton, C., Corley, W., and Sr., P. (1998). The Oklahoma City Bombing: structure and mechanisms of the Murrah Building. Journal of Performance of Constructed Facilities, 12(3), 120–136.

Su, Y., Tian, Y., & Song, X. (2009). Progressive collapse resistance of axially-restrained frame beams. ACI Structural Journal, 106(5), 600.

Talaat, M., & Mosalam, K. M. (2009). Modeling progressive collapse in reinforced concrete buildings using direct element removal. Earthquake Engineering & Structural Dynamics,

38(5), 609-634.

Yi, W. J., He, Q. F., Xiao, Y., and Kunnath, S. K. (2008). Experimental study on progressive collapse-resistant behavior of reinforced concrete frame structures. ACI Struct. J., 105(4), 433-439.

Yu, J., & Tan, K. H. (2012). Structural behavior of RC beam-column sub-assemblages under a middle column removal scenario. Journal of Structural Engineering, 139(2), 233-250.

Yu, J., & Tan, K. H. (2013). Special detailing techniques to improve structural resistance against progressive collapse. Journal of Structural Engineering, 140(3), 04013077.

Yu, J., & Tan, K. H. (2014). Analytical model for the capacity of compressive arch action of reinforced concrete sub-assemblages.

Appendix A

A set of 50 tests considering mid-column removal scenario are collected from various literatures, and among these tests there specimens.

Table A1. Summary of beam specimens.

Reference	No.	Specimen	Boundary stiffness / kN/m[*1]	Beam section		Total length	Longitudinal reinforcement			Material p	
				Height	Width		Top	Middle	Bottom	f_c(cylinder) /MPa	
				h/mm	b/mm	l/mm					
Ren et al. 2016	1	B1	Not given	170	85	4000	2T8+1T6	/	2T8	35.20	390
	2	B3	Not given	200	85	4000	2T8+1T6	/	2T8	35.20	390
Su et al. 2009	3	A1	1×10^6	300	150	2700	2T12	/	2T12	25.84	
	4	A2	1×10^6	300	150	2700	3T12	/	3T12	28.24	
	5	A3	1×10^6	300	150	2700	3T14	/	3T14	31.20	
	6	A4	1×10^6	300	150	2700	2T12	/	1T14	23.04	350
	7	A5	1×10^6	300	150	2700	3T12	/	2T12	26.48	
	8	A6	1×10^6	300	150	2700	3T14	/	2T14	28.64	
	9	B1	1×10^6	300	150	4200	3T14	/	3T14	18.56	
	10	B2	1×10^6	300	150	5700	3T14	/	3T14	19.28	
	11	B3	1×10^6	300	150	5700	3T14	/	2T14	21.12	
	12	C1	1×10^6	200	100	2700	2T12	/	2T12	15.92	
	13	C2	1×10^6	200	100	2700	2T12	/	2T12	16.80	
	14	C3	1×10^6	200	100	2700	2T12	/	2T12	16.32	
Chen et al. 2010	15	KLJ-3	1.375×10^6	290	145	2700	2T12	/	1T14	25.20	354
	16	KLJ-6	1.375×10^6	305	160	2700	3T12	/	3T14	24.88	354
	17	KLJ-9	1.375×10^6	294	144	2700	3T14	/	2T20	28.80	341
Niu et al. 2011	18	FA1	Not given	300	150	5700	2T14	/	2T14	15.85	
	19	FB1	Not given	300	150	5700	3T14	/	2T14	12.57	
	20	FB2	Not given	300	150	5700	3T14	/	3T14	15.95	

	21	FC1	Not given	300	150	5700	3T16	/	2T16	13.74	
	22	FC2	Not given	300	150	5700	3T16	/	3T16	13.73	
Yu & Tan 2013a	23	S1	1.06×10^5	250	150	5750	2T10+1T13	/	2T10	31.20	
	24	S2	1.06×10^5	250	150	5750	3T10	/	2T10	31.20	
	25	S3	4.29×10^5	250	150	5750	3T13	/	2T10	38.20	511
	26	S4	4.29×10^5	250	150	5750	3T13	/	2T13	38.20	
	27	S5	4.29×10^5	250	150	5750	3T13	/	3T13	38.20	
	28	S6	4.29×10^5	250	150	5750	3T16	/	2T13	38.20	494
	29	S7	4.29×10^5	250	150	4550	3T13	/	2T13	38.20	
	30	S8	4.29×10^5	250	150	3350	3T13	/	2T13	38.20	
Yu & Tan 2013b	31	F1-CD	4.29×10^5	250	150	5750	3T13	/	2T13	27.54	
	32	F2-MR	4.29×10^5	250	150	5750	3T13	/	2T13	27.54	
Sasani et al. 2011	33	P1	Not given	190	190	4170	5T9.5	/	2T9.5	41.00	
Qian et al. 2014	34	P1	Not given	180	100	4000	2T10	/	2T10	19.90	
	35	P2	Not given	140	80	2800	2T10	/	2T10	20.80	
FarhangVesali et al. 2013	36	1	Not given	180	180	4400	2T10	/	2T10	30.50	
	37	2	Not given	180	180	4400	2T10	/	2T10	27.00	
	38	3	Not given	180	180	4400	2T10	/	2T10	30.00	
	39	4	Not given	180	180	4400	3T10	/	3T10	26.00	
	40	5	Not given	180	180	4400	3T10	/	3T10	29.50	
	41	6	Not given	180	180	4400	3T10	/	3T10	30.00	
Alogla et al. 2016	42	SS1	1×10^5	250	`150	5750	3T10	/	2T10	19.35	
	43	SS2	1×10^5	250	150	5750	3T10	2T10	2T10	19.35	
	44	SS3	1×10^5	250	150	5750	3T10	2T10	2T10	19.86	
	45	SS4	1×10^5	250	150	5750	3T10	2T10	2T10	19.86	

Note: [*1] The boundary stiffness is used to calculate the boundary movement *t*, which is required in Eqs. 2-3 in the Park method.

Table A2. Summary of beam-slab specimens.

Reference	Specimen	Beam section		Beam reinforcement		Slab section		Slab reinforcement			Mate
								Longitudinal/ transverse		*l*/ mm	f_c(cylinder) MPa
		h/mm[*1]	b_b/mm	Top	Bottom	h_f/mm	b_f/mm	Top	Bottom		
Ren et al. 2016	S6	170	85	2T8+1T6	2T8	50	2000	T6@190	T6@190	4000	35.20
	S2	170	85	2T8+1T6	2T8	50	685	T6@190	T6@190	4000	35.20
	S3	200	85	2T8+1T6	2T8	50	2000	T6@190	T6@190	4000	35.20
	S4	170	85	3T10	2T10	50	2000	T6@190	T6@190	4000	35.20
	S5	170	85	2T8+1T6	2T8	75	2000	T6@160	T6@160	4000	35.20

Note: [*1] The meanings of *h*/ b_b/ h_f and b_f are given in Fig 7.

Appendix B

Detailed calculation procedure of the beam-slab specimen (Specimen S6 of Ren et al. (2016)).